CrossMark

Application of FDS to Under-Ventilated Enclosure Fires with External Flaming

Guoxiang Zhao*, Tarek Beji and Bart Merci, Department of Flow, Heat and Combustion Mechanics, Ghent University, Sint-Pietersnieuwstraat 41, 9000 Ghent, Belgium

Abstract. Numerical simulations are conducted to investigate the accuracy of the fire dynamics simulator (FDS 6.0.1) for under-ventilated enclosure fires with external flaming. The accuracy is discussed first in terms of mass balance at the steady-state stage for the enclosure volume. The required fineness of the grid is determined by analyzing the mass balance using two non-dimensional length scales. The first considers the ratio of the ventilation factor to the grid cell size, and the second considers the ratio of the hydraulic diameter of the opening to the grid cell size. When these two length scales are larger than 10, the corresponding mass balance error as obtained from post-processing the output is lower than 4%. The simulation results, including flow through the vertical opening, heat release rate inside the enclosure, gas temperature inside the enclosure, neutral plane height, and external flame height are compared with experimental data and empirical correlations. The air inflow rate through the opening is found to correlate linearly to the ventilation factor as $\dot{m} = 0.41 \cdot A\sqrt{H}$. For the heat release rate inside the enclosure, the predictions follow the empirical correlation $\dot{Q}_{in} = 1131 \cdot A\sqrt{H}$. This is directly related to the air inflow rate and incomplete combustion with the inflowing oxygen. Time-averaged gas temperatures inside the enclosure are under-predicted by maximum 13.1% compared with experimental data at the corner near the opening. Neutral plane height values at the opening, determined from the velocity profile of the vent flow, show good agreement with empirical estimations ($Z_f = 0.4 \cdot H$). Two methods are employed to determine the external flame height, namely a temperature based method and a volume heat release rate based method. The trends are captured correctly.

Keywords: Under-ventilated fire, FDS, Ventilation factor, External flaming, Numerical simulations

List of Symbols

A	Area of the opening (m^2)
W	Width of the opening (m)
H	Height of the opening (m)
H_N	Height of the neutral plane (m)
$\dot{Q}$	Total heat release rate of fire (kW)
$\dot{Q}_{in}$	Heat release rate inside the enclosure (kW)
$\dot{Q}_{ext}$	Heat release rate burning outside the enclosure (kW)
Z_f	Mean flame height from location of the neutral plane height (m)
ℓ_1	Length scale ratio based on the opening geometry (−)

---

* Correspondence should be addressed to: Guoxiang Zhao, E-mail: guoxiang.zhao@ugent.be

c_p	Specific heat (kJ/(kg.K))
T_∞	Ambient temperature (K)
g	Gravitational acceleration (m/s^2)
T_g	Gas temperature (K)
ℓ_1^*	Length scale ratio based on the opening geometry and the simulation grid size (−)
ℓ_2^*	Length scale ratio based on the hydraulic diameter and the simulation grid size (−)
$\dot{m}_{in}$	Mass inflow rate through the opening (kg/s)
$\dot{m}_{out}$	Mass outflow rate through the opening (kg/s)
$\dot{m}_{fuel}$	Mass supply rate of the fire source (kg/s)
D_h	Hydraulic diameter of the opening (m)

Greek

ΔH_{air}	Heat of combustion per kg air consumed (kJ/kg)
ρ_∞	Density of gas (kg/m^3)
ε	Mass balance error (−)
δ_x	Simulation grid size (m)

1. Introduction

In recent years, fire safety of high-rise building fires has attracted extensive attention, especially in cases where flames are ejected from an enclosure and attached to building's façade. The ejected flames can potentially cause secondary fires which might spread from the original floor to upper floors, as well as to adjacent buildings. Therefore, it is necessary to understand the physics involved and provide reliable predictions of the fire dynamics in such scenarios.

The main heat transfer mechanisms involved are radiation and convection. Their contributions are affected mainly by the ejected flame height and its temperature profile. The extent of external flaming depends on the excess fuel, i.e., fuel that is not burned inside the enclosure as a consequence of limited ventilation [1, 2]. The latter depends on the opening size (i.e., ventilation factor).

In an under-ventilated fire, the combustion inside the enclosure is limited by the mass flow rate of air that can enter through the openings. Part of these openings is occupied by hot gases leaving the enclosure. If the air inflow is insufficient for all combustible gases to burn inside the enclosure, flames extend out of the enclosure and combustion takes place where the hot unburned gases mix with air outside. Understandably, a lot of effort has been devoted to study this subject by means of theoretical analysis, experimental investigation and numerical modelling (e.g., [1–12]).

The air inflow through the enclosure is governed by the pressure differences between the two sides of the opening. As a result, the flows at the opening are bi-directional with cool air inflow in the lower part and hot smoke outflow in the upper part. Based on Bernoulli's equation, the air inflow rate $\dot{m}_{air}$, is found to be, in well-mixed conditions, proportional to the ventilation factor $A\sqrt{H}$ [1, 13–15]:

$$\dot{m}_{air} = C \cdot A\sqrt{H} \text{ in kg/s} \tag{1}$$

where A (m^2) and H(m) are respectively the area and height of the opening, and C is a constant determined by the opening discharge coefficient and gravitational acceleration constant. Different values for C have been reported in the literature (e.g. [15–17]). Thomas and Heselden [16] estimate the value of this constant at 0.5 $kg/s \cdot m^{5/2}$, which is the value most commonly found in the literature. Computational fluid dynamics (CFD) techniques have also been applied to simulate the doorway flow induced by an enclosure fire, using various CFD codes [18, 16, 19–22]. FDS has been developed and is maintained by the National Institute of Standards and Technology (NIST) [23, 24]. In [21], a value of 0.47 for C was derived from FDS (version 3.0.1) simulation while the experimental value was 0.46, which indicates that FDS is capable of predicting the mass flow rate through the ventilation opening.

The upper limit for the HRR inside the enclosure can be determined, assuming that all the incoming air through the vent is consumed in the combustion. Indeed, the maximum heat release rate (HRR) inside the enclosure is found by multiplying the air inflow rate with the heat of combustion per unit mass of air ($\Delta H_{air} \approx 3000$ kJ/kg):

$$\dot{Q}_{in} = C \cdot \Delta H_{air} \cdot A\sqrt{H} \text{ in kW} \tag{2}$$

Taking $C = 0.5 kg/s \cdot m^{5/2}$, Eq. (2) becomes $\dot{Q}_{in} = 1500 \cdot A\sqrt{H}$. It should be noted that in cases with external flaming, the exact HRR inside the enclosure cannot be determined directly in experiments. Indeed, in most experiments, the heat release rates are measured based on two methods: either from the mass loss rate of the burner, or by means of oxygen consumption method collecting gases. Neither of these methods provides the exact HRR generated inside the enclosure since part of the combustion occurs outside the enclosure. In [6, 7] a plateau in the evolution of the total heat release rate equal to $1500 \cdot A\sqrt{H}$ was observed for several configurations with under-ventilated conditions prior to external flaming. This plateau value provides an estimate for the HRR inside the enclosure, although it is not guaranteed that the value does not change during the external flaming period, since it is not guaranteed that the same amount of oxygen is consumed per unit time inside the enclosure, given changes in e.g. the flow field.

As a merit of CFD techniques, the heat release rate in a predefined domain can be determined by integrating the Heat Release Rate per Unit Volume (HRRPUV) over that domain [Such post–post-processing is readily available in FDS which is used in the present paper (version 6.0.1)]. This enables us to numerically study the relationship between the heat release rate and the opening size.

Several methods have also been developed, based on experimental data and theoretical analysis, for predicting temperatures in enclosure fires during the fully developed fire stage [25]. Babrauskas [12, 26] proposed a method based on the energy balance in the enclosure system, which involves terms take heat released per unit time within the enclosure, heat losses through openings by radiation and convection and conduction into the walls, floor and ceiling. This method is summarized by Walton and Thomas in [25].

Moreover, numerical methods have also been used to predict the gas temperature. It should be noted that a prerequisite for accurately predicting the gas temperature is accurate modeling of the combustion in under-ventilated fires. This, however, is still a challenge for the fire safety community, although progress is made through several studies, dedicated to develop models or theoretical analysis for incomplete combustion and flame extinction (e.g., [27–30]).

Charge coupled device (CCD) cameras are commonly used for recording the external flaming. Using a probabilistic based method to post-process the video footage [31], the flame height value can be determined. This method was employed in previous experimental studies (e.g., [6, 7, 28]). The key parameters in the prediction of the flame shape are the amount of excess heat release rate, the opening geometry, and the atmospheric conditions (e.g., wind). Some theoretical models (e.g., [32–34]) and correlations [6, 7] have been developed,based on experimental data. Only few attempts [35, 36] can be found in the literature to numerically study the height of the flame ejected from the opening of an under-ventilated enclosure fire.

This paper aims to assess simulation results obtained with of FDS (version 6.0.1) for the under-ventilated enclosure fire and external flaming based on a set of experimental data [6, 7]. Various opening geometries and a single inert façade wall are considered. The discussion of simulation results includes the vent flows through the opening, time-averaged gas temperature, HRR inside the enclosure, neutral plane height, and external flame height.

2. Numerical Simulations

2.1. Brief Description of the Simulation Settings

As is mentioned in previous section, FDS is employed in this work. Whereas details are found in [24], a brief description of the settings is described here. In FDS (version 6.0.1), the Navier–Stokes equations are solved using a second order finite difference numerical scheme with a low-Mach number formulation. The turbulence model is based on Large Eddy Simulation (LES). Four models can be chosen for the subgrid-scale turbulent viscosity, with the 'modified Deardorff' as default model. FDS uses a combustion model based on the mixing-limited, infinitely fast reaction of lumped species. Lumped species are reacting scalar quantities that represent a mixture of species. A simple extinction model has been implemented in FDS, which is based on a critical flame temperature value (T_{LFL}). In cells where the temperature drops below this T_{LFL} value, combustion does not continue since the released energy cannot raise the temperature above the value for combustion to occur. A critical flame temperature 1427°C has been used in the present study with a propane burner, according to [24]. The Radiative Transfer Equation (RTE) is solved using the finite volume method (FVM). A radiation fraction of 0.35 is prescribed as a lower bound in order to limit the uncertainties in the radiation calculation induced by uncertainties in the temperature field.

Heat losses to the walls are calculated by solving the 1-D Fourier's equation for conduction. In the present study, the default models and constants in FDS are applied. The reader is referred to [24] for more detail.

2.2. Simulation Details

The set-up in the modelling corresponds to the experiments reported in [6, 7]. The enclosure dimensions are 0.5 m × 0.5 m × 0.5 m. A fiberboard plate serves as external façade wall, as shown in Figure 1. By setting various widths and heights of the opening, under-ventilated conditions has been obtained. A 0.1 m × 0.2 m propane burner provides a fire source with a specific theoretical heat release rate inside the enclosure. The burner is located at the center of the enclosure. All walls, including the façade wall, consist of fiberboard with the following proper-ties: the thickness is 0.025 m, the density is 350 kg/m³, the thermal conductivity is 0.3 $W/m \cdot K$, the emissivity is 0.9, and the heat capacity is 1700 $J/kg \cdot K$. A more detailed description of this experimental work can be found in [6, 7].

Four different opening geometries are considered: 0.1 m × 0.2 m, 0.2 m × 0.2 m, 0.2 m × 0.3 m, and 0.3 m × 0.3 m. The computational domain has been extended by 50 cm outside the enclosure, as shown in Figure 2a, in order to limit the influence of the 'open' boundary condition on the flow field. As shown in Figure 2b, two meshes are used within the simulation domain. The first mesh contains the entire enclosure and the lower part of the outdoor domain, and the second mesh covers the rest of the domain. The obstructions in the FDS model are made thick (at least one grid cell thick).

As shown in previous studies [37–41], FDS simulation results are sensitive to grid size. Smaller grid cells are generally preferred for more accurate simulations.
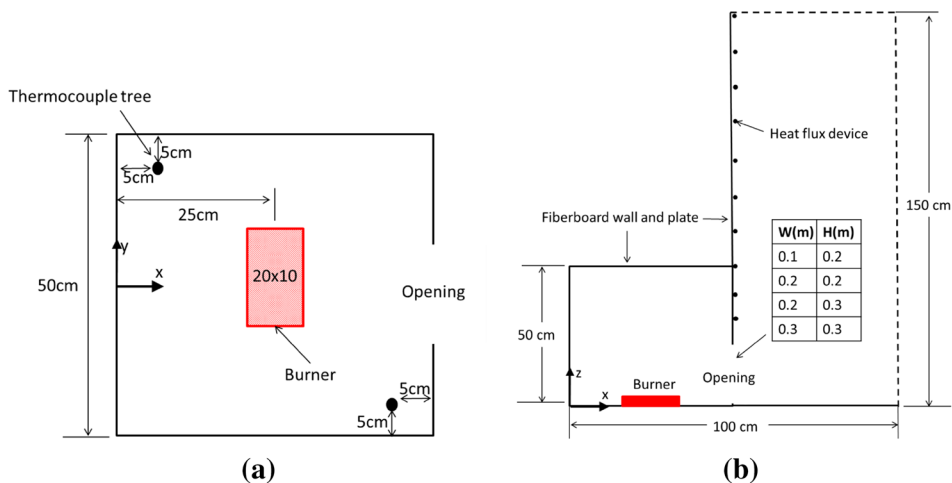
Figure 1. **Sketch of the experimental set-up. a** *Top view* **of the enclo-sure. b** *Side view* **of the enclosure.**

(a)   **(b)**
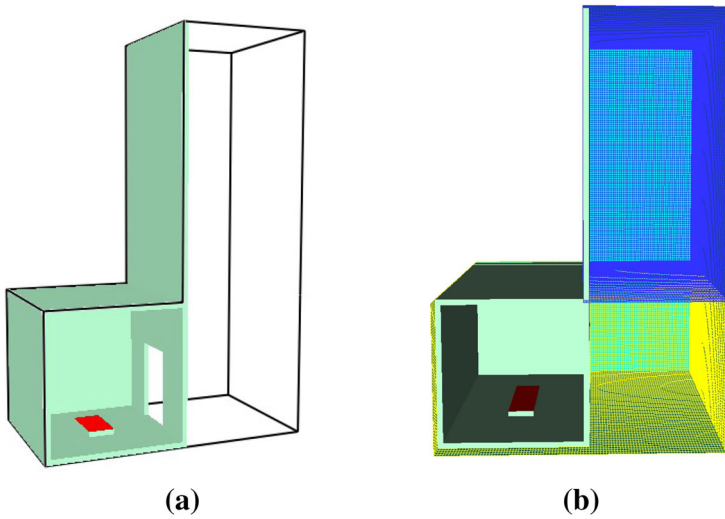
Figure 2. Snapshots of the simulation domain and meshes. a Global view of simulation domain. b Two meshes in the domain.

However, such simulations will also be more expensive in terms of computational cost and storage requirement. Therefore, it is necessary to discuss the required grid resolution for the present study.

In case of enclosure fires with external flaming, both the fire source and the vent flow need careful consideration. For the fire source, a characteristic length scale D^* is related to the total heat release rate $\dot{Q}$ by the following relation [37]:

$$D^* = \left[\frac{\dot{Q}}{\rho_\infty C_\infty T_\infty \sqrt{g}}\right]^{2/5} \tag{3}$$

In Eq. (3), $\dot{Q}$, ρ_∞, C_∞, T_∞, and g are respectively the total heat release rate (kW), the density at atmosphere gas (kg/m^3), the specific heat of air $(kJ/kg \cdot K)$, the atmosphere temperature (K), and the gravity acceleration (m/s^2). McGrattan [42] suggested a cell size of 10% of the plume characteristic length D^* as adequate resolution, based on careful comparisons with plume correlations. Based on this '10% criterion', the required cell size for a HRR between 30 kW and 90 kW, is in the range of 2.3 cm to 3.6 cm.

Besides the length scale concerning the fire source, it is also necessary to examine other length scales, concerning the accurate simulation of the flow through the opening. However, this length scale has not been considered systematically in previous numerical studies. The discussion is presented in Sect. 3.1.

In this study, cell sizes of 1, 2 and 4 are used for each opening geometry. In order to get under-ventilated conditions, all the heat release rates of the burner

Table 1
List of Simulations

Opening geometry		$\dot{Q}_{in}$ (Eq. 2) (kW)	Fire source HRR $\dot{Q}$ (kW)	Grid size (cm)	Case no.
W (m)	H (m)				
0.1	0.2	13.42	30	4,2,1	1–3
0.1	0.2	13.42	40	4,2,1	4–6
0.2	0.2	26.83	50	4,2,1	7–9
0.2	0.2	26.83	60	4,2,1	10–12
0.2	0.2	26.83	70	4,2,1	13–15
0.2	0.3	49.30	60	4,2,1	16–18
0.2	0.3	49.30	70	4,2,1	19–21
0.2	0.3	49.30	80	4,2,1	22–24
0.3	0.3	73.94	80	4,2,1	25–27
0.3	0.3	73.94	90	4,2,1	28–30
0.2	0.2	26.83	30,40	1	31,32

are set to be larger than the value of $1500 \cdot A\sqrt{H}$. Table 1 shows a list of all 32 simulations.

In case 27, for example, each cell has dimensions of 0.01 m × 0.01 m × 0.01 m, and the total number of cells in the computational domain is $(102 \times 60 \times 54) + (50 \times 60 \times 100) = 630,000$. The time step is 0.00112 s, set automatically during the FDS calculation by dividing the mesh size by the characteristic velocity of the flow. The total simulation duration is set to 20 min, as steady state conditions are reached after 8 min (see later). For these two meshes of the simulation domain, two computing processors (2.6 GHz CPU with 32 GB RAM) were used. This computation takes about 144 h. The simulation results discussed in the following sections are mean values, averaged during the period from 500 s to 1200 s.

2.3. Measurement Devices

The mass inflow and outflow rates through the opening have been determined in FDS by setting two measurement devices at the level of the doorway called "Mass Flow +" and "Mass Flow −". The actual heat release rate inside the enclosure has been determined by integrating the heat release rate per unit volume "HRRPUV". Gas temperature inside the enclosure has been determined in two opposite corners (see Figure 1) at several heights from floor level (Z = 0.04, 0.09, 0.14, 0.19, 0.24, 0.29, 0.34, 0.39, 0.44, and 0.49 m). In this work, two different methods have been considered to determine the flame height. The first method uses a temperature reference value to define the flame tip in the center plane (y = 0). The flame tip position is taken as the highest location outside the room volume where the time-averaged mean temperature is T = 520°C (i.e., $\Delta T = 500°C$ compared to ambient) [43]. The reference level for the definition of the flame height is taken as the neutral plane height (see Figure 3), as indicated in
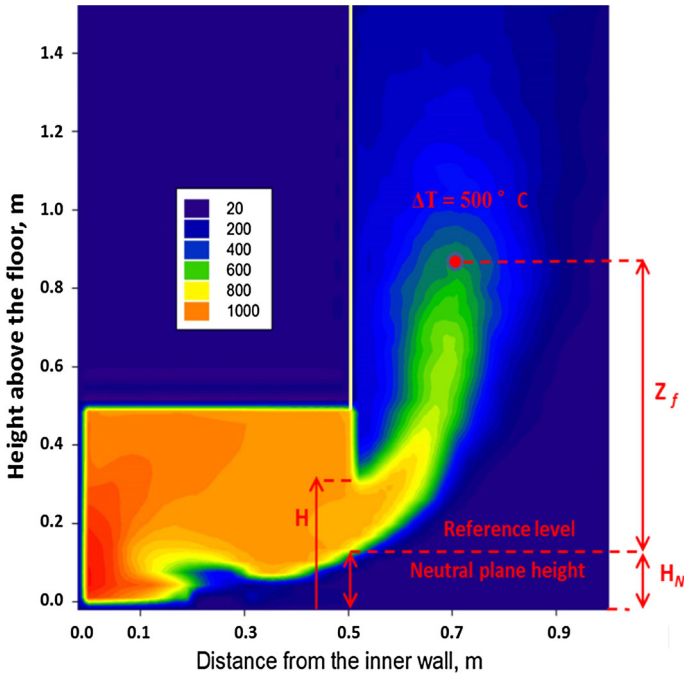
Figure 3.   Time-averaged temperature contour plot showing the flame tip position and neutral plane height.

[6, 7]. In the second method, the flame tip is determined from the heat release rate per unit volume (HRRPUV) of the flame.

3. Simulation Results and Discussion

Since the mass flow rate of air entering the enclosure is not sufficient for complete combustion of the imposed total HRR, the combustible gases leave the compartment. They find fresh air and react outside the enclosure. Figure 4 provides a typical snapshot showing external flaming in the simulation.

Figure 5 shows the time evolution of mass flow rates through the ventilation opening for case 27. The outflow rate, inflow rate, fuel flow rate, and net flow (the difference between the outflow and inflow), as obtained from post-processing, are approximately constant during most of the time after the ignition, with an average value of 0.0222 kg/s, 0.0201 kg/s, 0.0017 kg/s, and 0.0020 kg/s respectively. The difference between the net mass flow rate and the fuel mass flow rate is discussed in detail in Sect. 3.1.

Figure 6 shows the temporal evolution of temperatures at several heights for case 27 (see Table 1). These temperatures were recorded by the back corner thermocouple tree (see Figure 1a). It is seen that a quasi-steady state condition has
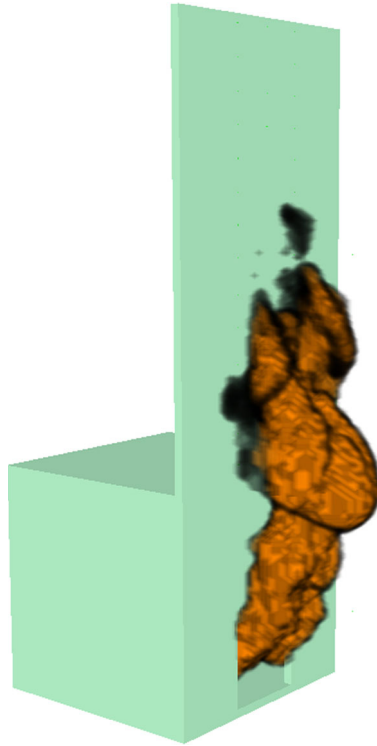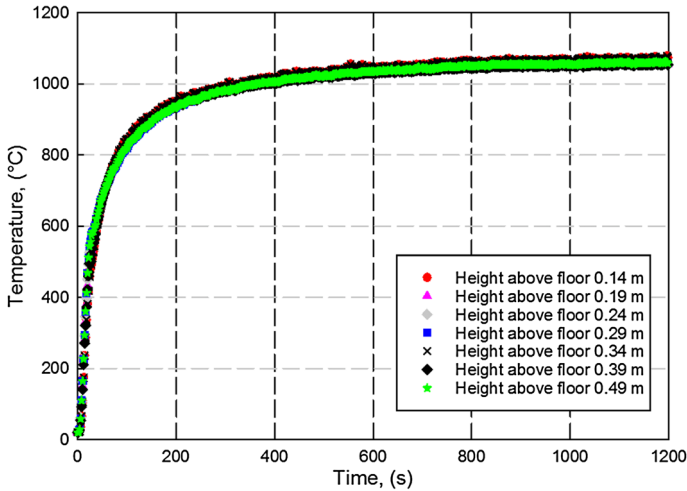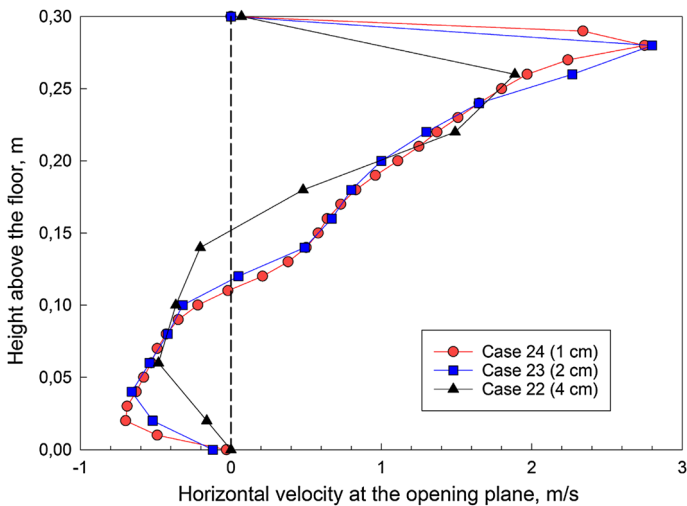
Figure 4.   Snapshot showing a typical external flaming in the simulation.
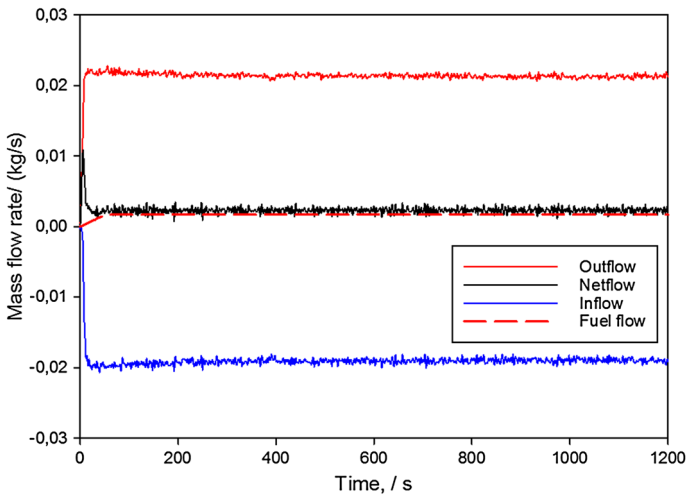
Figure 5.   Temporal evolution of mass flow rate through the ventilation opening for case 27 (see Table 1).
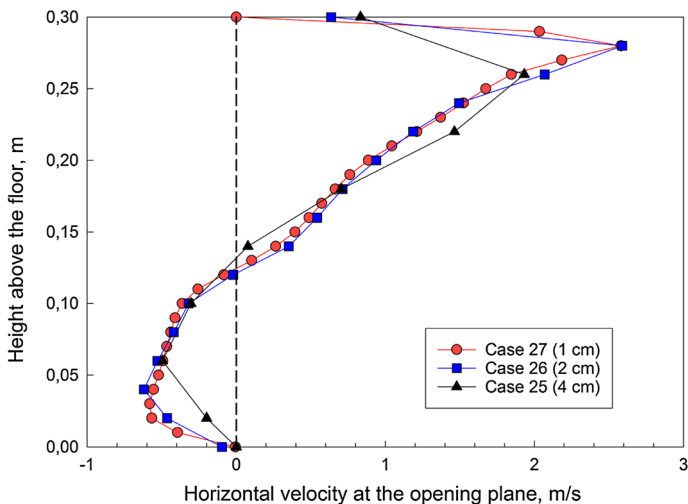
**Figure 6. Temporal evolution of temperatures at the back corner for case 27 (see Table 1).**

Figure 7. Cell size effect on horizontal velocity along the centerline of the opening for cases 22–24 (see Table 1).

been obtained in the simulation roughly from 500 s to 1200 s. The other cases show a similar trend.

The dependence of CFD simulation results on the grid size is studied first, focusing on the flow through the opening. Figures 7, 8, 9, and 10 show, respectively, the steady state horizontal velocity and temperature along the vertical cen-
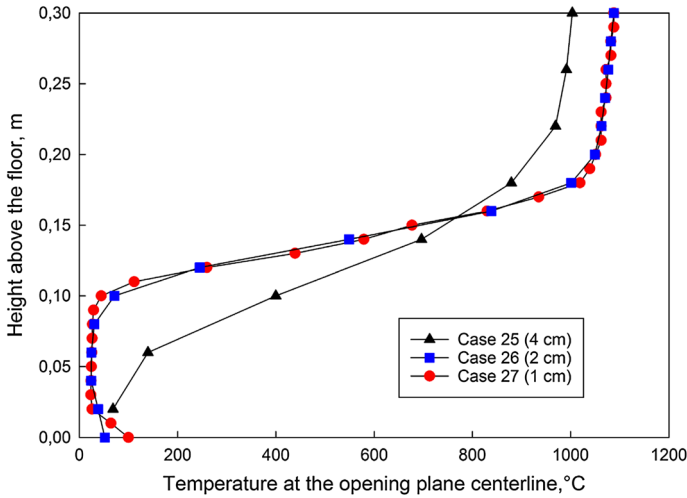
Figure 8.   Cell size effect on horizontal velocity along the centerline of the opening for cases 25–27 (see Table 1).
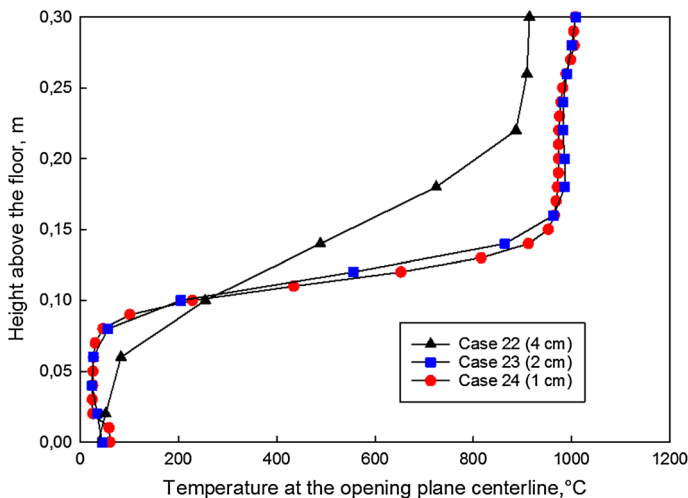
Figure 9.   Cell size effect on temperature along the centerline of the opening for cases 22–24 (see Table 1).

terline of the opening for cases 22, 23, 24 (cell sizes 4, 2 and 1) and cases 25, 26, 27 (cell sizes 4, 2 and 1). Similar trends were observed for the other cases. A 2 cm cell size or finer is sufficient to ensure the grid insensitivity of the simulation results.

Figure 10. Cell size effect on temperature along the centerline of the opening for cases 25–27 (see Table 1).

At a certain height at the opening, the horizontal velocity is zero. This height is called the 'neutral plane height'. The neutral plane height value is determined as the position where the horizontal velocity profile crosses the dashed line (Figures 7, 8) for all cases.

3.1. Flow Through the Opening

First, the mass inflow rate of air through the opening is discussed. The mass inflow rates for cases with 1 cm grid size for the four different ventilation factors are presented in Figure 11. Not surprisingly, a linear correlation is observed between the mass inflow rate and ventilation factor: $\dot{m} = C \cdot A\sqrt{H}$. The constant coefficient C is roughly 0.41. This is at the lower end of the range 0.4–0.61 found in the literature [15].

The prediction of the air mass flow rate through the opening in under-ventilated conditions is of great importance, because it determines the extent of burning inside and outside the enclosure. The required fineness of the grid was already illustrated in Figures 7 and 8. In addition hereto, we discuss grid convergence in terms of a mass balance 'error' (Eq. 7), based on post-processing of output data, using two length scales ratios. The first one considers the ratio of the ventilation factor to the grid cell size:

$$\ell_1^* = \ell_1/\delta_x = (A\sqrt{H})^{2/5}/\delta_x \tag{4}$$

This length scale ratio varies from 3.78 to 40 for the cases considered according to the value of the grid size and the opening geometry.
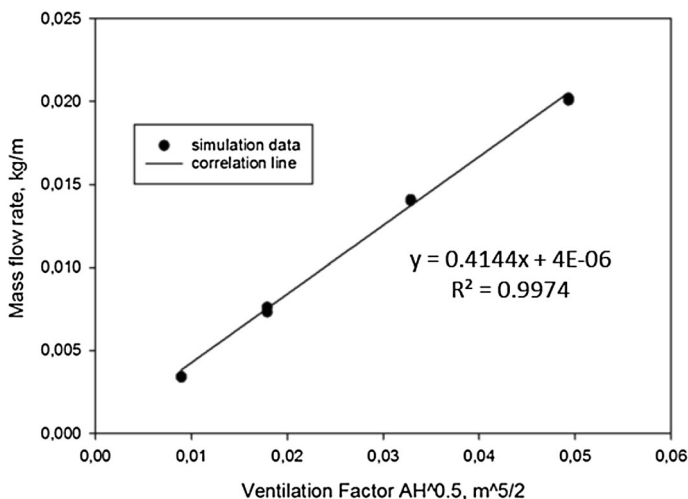
Figure 11. The correlation between mass inflow rate and the venti-lation factor for 1 cm grid size results.

The second one considers the ratio of the hydraulic diameter of the opening to the grid cell size:

$$\ell_2^* = D_h/\delta_x = (2W \cdot H/(W + H))/\delta_x \tag{5}$$

This length scale ratio varies from 3.33 to 40 for the cases considered according to the value of the grid size and the opening geometry.

At steady-state conditions, the mass balance applied to the enclosure volume reads:

$$\dot{m}_{out} = \dot{m}_{in} + \dot{m}_{fuel} \tag{6}$$

where $\dot{m}_{out}$ is the total air mass outflow rate through the opening (kg/s), $\dot{m}_{in}$ is the total air mass inflow rate through the opening (kg/s), $\dot{m}_{fuel}$ is the mass supply rate of the fire source (kg/s). Here a mass balance 'error' is defined as the following:

$$\varepsilon = \left| 1 - \frac{\dot{m}_{in} + \dot{m}_{fuel}}{\dot{m}_{out}} \right| \times 100\% \tag{7}$$

It is stressed that this is not a real 'error' at the level of implementation. The discussion of Figures 12 and 13 is based output values as obtained from post-processing. The implementation in FDS at the level of discretization differs from what is delivered as output. This is discussed in more detail below, but the reader must beware of this issue already now, since true errors in mass balance of more than 1% would already be unacceptable.
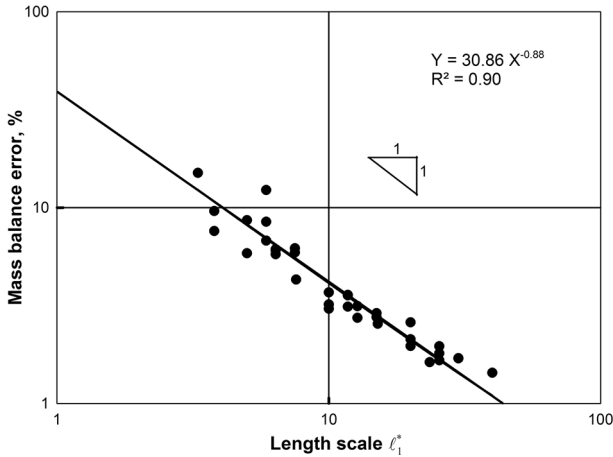
Figure 12. Mass balance 'error' ε (Eq. 7) based on post-processing of output data for all the cases analyzed using length scale ℓ_1^*.
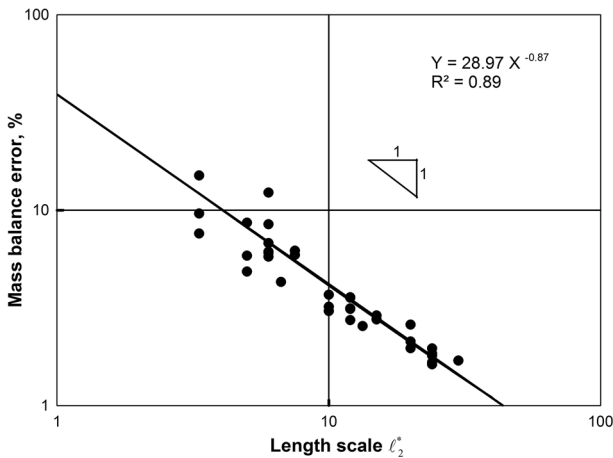
Figure 13. Mass balance 'error' ε (Eq. 7) based on post-processing of output data for all the cases analyzed using length scale ℓ_2^*.

Figure 12 shows that ε varies from 1.4% to 15.0%. It is almost inversely proportional to ℓ_1^*. Like the 10% criterion when choosing cell size for fire plume, a value of 10 is chosen for ℓ_1^*. For $\ell_1^* \geq 10$, ε reduces to values below 4%. Such an approach can be used to estimate opening uncertainties associated with the grid size in the prediction of flows through. In the following sections, only the cases with $\ell_1^* \geq 10$ are used for the analyses. The cell sizes used in these cases are smaller than or equal to 2 cm.

Figure 13 presents ε using ℓ_2^*. Similarly as in Figure 10, ε is almost inversely proportional to ℓ_2^*, and for $\ell_2^* \geq 10$, the mass balance error reduces to values below 4%.

As mentioned, it is stressed that Figures 12 and 13 refer to post-processing of output data. In the output, FDS uses a simple method to define the mass flux, which differs from what is implemented in the discretization of the mass conservation equation. The output quantities 'MASS FLOW +' and 'MASS FLOW -' are calculated as follows:

$$\dot{m} = \int \rho u \cdot dA \tag{8}$$

The velocity (u) is the component of velocity in the specified direction. The u-component of the velocity is defined directly in the measurement plane. The density (ρ) is the average of the densities at each side of the measurement plane. The area (A) is the sum of the areas of the cell faces. This form of the mass flow is thus approximate, because the mass transport equation uses a flux limiter to define the mass advection. Thus, the output 'MASS FLOW' is not exact, which is the reason why the non-zero mass balance error is obtained.

However, considering this issue, the method as described is still useful as criterion or indicator to determine the required grid resolution in simulations where flows through opening are crucial. In other words, the ℓ_1^* or ℓ_2^* criterion must be checked in addition to the D^* criterion.

Table 2 illustrates (for case 24) once more that ε is not a true error in mass balance at the level of implementation. Indeed, reducing 'velocity_tolerance' (which refers to possible errors at mesh interfaces) and increasing the maximum number of calls to the pressure solver (max_pressure_iterations) in the FDS input file, does not modify ε significantly.

Finally, note that the discussion of the grid convergence based on the mass balance 'error' is more informative than examining inflow or outflow rates directly. Indeed, the absolute values of such quantities depend on, e.g., the heat release rate and opening size (Figure 11). Consequently, relative deviations are not directly visible and moreover, in contrast to what has been presented in Figures 12 and 13, only 3 values for the length scale ratios can be used per case (since 3 levels of grid refinement have been used for each case).

Table 2
The Effect of 'Velocity Tolerance' and 'Max Pressure Iterations' on the Mass Balance Error for Case 24

No.	Velocity tolerance (m/s)	Max pressure iterations (−)	ε (%)
1(default)	–	10	2.7308
2	0.001	100	2.7294
3	0.0001	1000	2.7280

3.2. Heat Release Rate Inside the Enclosure

The averaged heat release rate inside the enclosure is presented in Figure 14. Four groups of data are observed, each of them corresponding to one value of the ventilation factor ($A\sqrt{H}$). As indicated in Figure 14, the predicted HRR inside the enclosure (HRR_{in}) shows a linear correlation with the ventilation factor. The linear regression coefficient is 1130.7 kW/m$^{5/2}$.

This is approximately 25% below the value 1500 kW/m$^{5/2}$ mentioned above in the empirical correlation. The deviation is mainly related to the air inflow rate and the completeness of the use of oxygen for combustion inside the enclosure. Note that the constant coefficient C derived from the simulation is 0.41, which is lower than 0.5 (which correspond to 1500 kW/m$^{5/2}$). This should already result in an 18% lower HRR inside. The remainder can be attributed to completeness of combustion.

Indeed, not all oxygen entering the compartment is entirely consumed by the combustion. Some air is immediately entrained into the exiting flow and does not participate in the combustion. In order to illustrate this, the net mass flow rate of oxygen through the opening for case 24 is outputted and shown in Figure 15. The average value between 500 s and 1200 s is 0.002528 kg/s. At the same time, the average mass flow rate for air entering the compartment is 0.013910 kg/s. Oxygen mass fraction in ambient air is 0.2323. Based on this, the maximum oxygen inflow rate is calculated to be 0.003231 kg/s. This is higher than the actual value 0.002528 kg/s of net oxygen flow rate. This difference implies that there is some oxygen flowing out of the compartment without participating in the combustion inside the enclosure.
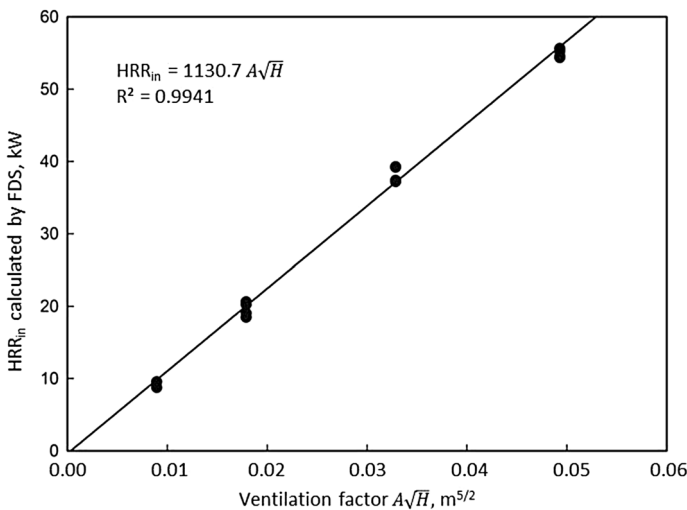
Figure 14.   Linear correlation between the ventilation factor and predicted HRR inside the enclosure HRR$_{in}$.
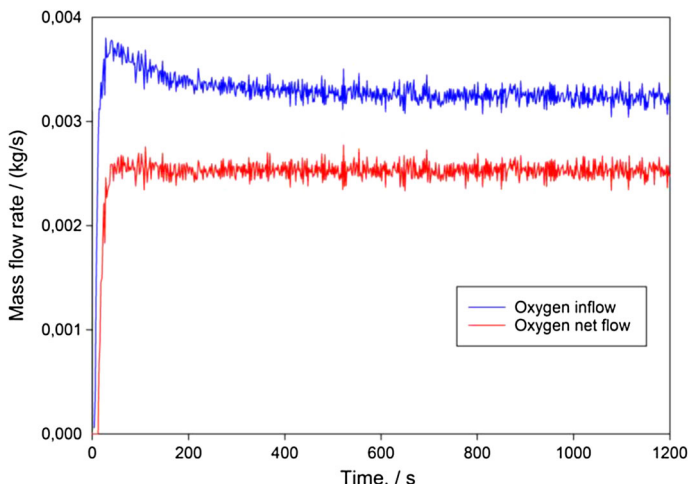
Figure 15. Temporal evolution of mass flow rate of oxygen through the opening for case 24 (see Table 1).

3.3. Gas Temperature Inside the Enclosure

In Figure 16, the vertical temperature distributions are presented, obtained from two thermocouples trees at two corners of the enclosure for different opening geometries. The temperatures at two opposite corners are similar, but not identical, revealing deviations from the perfectly mixed situation. Similar observation has been made before in [44]. However, deviations are not very large, so that it is meaningful to define an average temperature inside the enclosure.

Higher temperatures are observed in Figure 16 for higher ventilation factors, as less excess fuel leaves the compartment and HRR_{in} increases (Figure 14). Babrauskas' correlation [12, 26] can be used to compare with the simulation results of the average temperature inside the enclosure:

$$T_g = T_\infty + (T^* - T_\infty) \cdot \theta_1 \cdot \theta_2 \cdot \theta_3 \cdot \theta_4 \cdot \theta_5 \tag{9}$$

In Eq. (9), T^* is an empirical constant, set equal to 1725 K, and five factors account for different physical phenomena: the burning rate stoichiometry (θ_1), the wall steady-state losses (θ_2), the wall transient losses (θ_3), the opening height effect (θ_4), and the combustion efficiency (θ_5).

The five factors in correlation (9) can be determined from the material properties and the other parameters used in the simulation. Figure 17 shows the comparison between the predicted average temperatures and correlation (9). The relative differences are below 10% for all scenarios.

In Table 3, the time-averaged gas temperatures at the front corner are compared with experimental data for cases 8, 11, 31 and 32, which correspond to an opening size of 0.2 m × 0.2 m. As indicated in Figure 18, the gas temperatures at
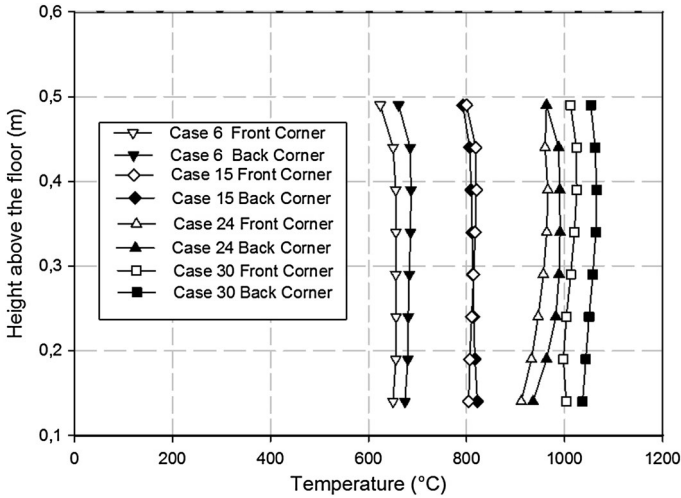
Figure 16. **Temperature distribution inside the enclosure obtained from *front* and *back corner* thermocouple trees for four different opening geometries. Case numbers: see Table 1. *Closed symbols* refer to simulation results in the *back corner*, while *open symbols* refer to results obtained in the *front corner* (see Figure 1).**
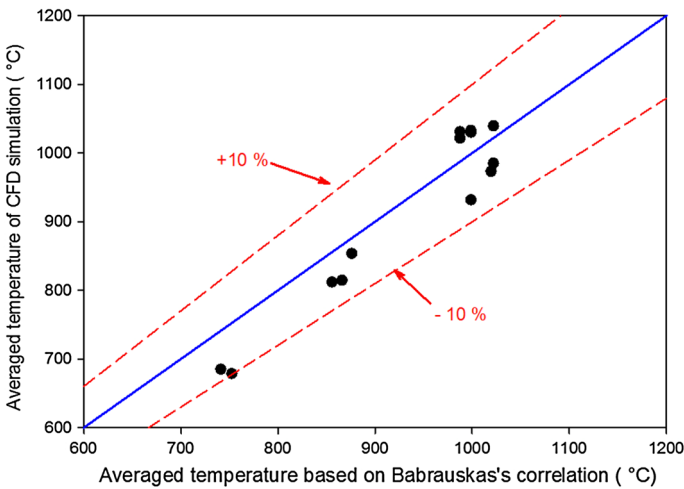
Figure 17. **Comparison of average temperatures obtained with FDS to correlation (9) [12, 26].**

Table 3
Comparisons of Gas Temperatures in Simulations and Experiments for Opening Size of 0.2 m × 0.2 m

| Case no.	HRR_{Total} (kW)	$T_{av\text{-}exp}$ (°C)	$T_{av\text{-}sim}$ (°C)	$(T_{av\text{-}exp} - T_{av\text{-}sim})/T_{av\text{-}exp}$ (%)
11	60	967 ± 16.4	842.1 ± 12.6	12.9
8	50	946 ± 19.0	823.1 ± 11.6	13.0
31	40	928 ± 6.6	805.7 ± 11.7	13.1
32	30	900 ± 5.9	799.9 ± 3.4	12.0
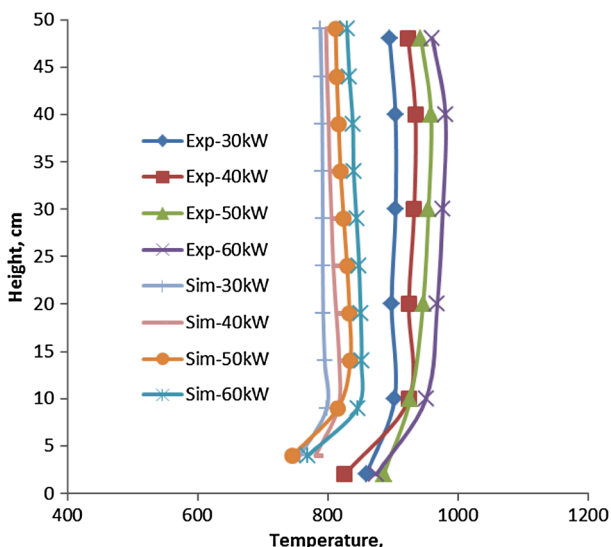
Figure 18.   Comparison of average temperatures obtained with FDS to experimental data for cases 8, 11, 31, and 32 (see Table 1).

heights of 10 cm or more above the floor are approximately uniform. Their average values are present in Table 3. The deviations from the average value are presented in this table as well.

   In general, the simulation results under-predict temperature, but deviations are less than 13.1%. This is not surprising, taking into account the possible under prediction of heat release rate inside the enclosure as mentioned above. Also this could be related to the fact that no radiation correction has been performed on the experimental data.

3.4. Flame Heights Outside the Enclosure

In [11], the neutral plane height is estimated to be at a distance $0.4H$ from the bottom of the opening, with H the opening height. Figure 19 presents the com-
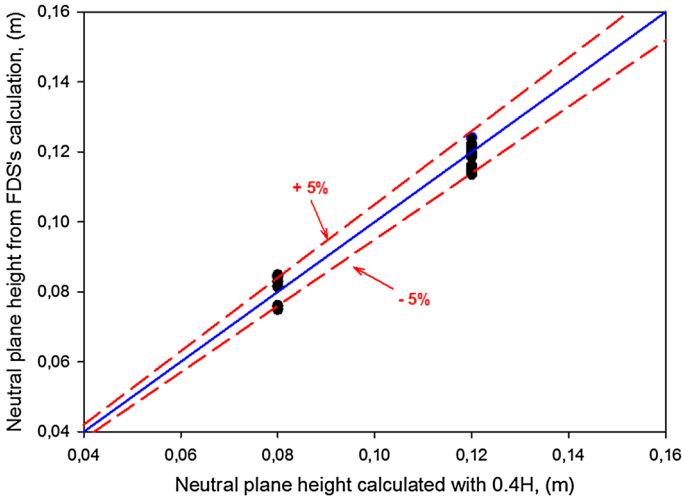
Figure 19.   Comparison of neutral plane height as obtained from the simulation to the neutral plane height from empirical estimations (0.4 *H*) [9].

parison of the neutral plane heights obtained from the simulation to the value from empirical estimations (0.4*H*). Agreement is clearly good (deviations <5%).

As mentioned in Sect. 2.3, two different methods have been used in the post-processing of the simulation results to determine the flame height. The first one is based on a temperature reference value (520°C [43]) to define the flame tip. The second method is based on the heat release rate per unit volume (HRRPUV) of the flame. In this work, two reference values of HRRPUV are considered, namely 0.5 MW/m^3 [45] and 1.2 MW/m^3 [46]. In other words, as long as the HRRPUV exceeds 0.5 MW/m^3 or 1.2 MW/m^3, a flame is supposed to be present. Results for cases 8, 11, 31, and 32 are presented in Table 4. Note that the flame height is calculated from the neutral plane height.

For the same ventilation factor, the amount of fuel consumed inside the enclosure should remain approximately the same. For a higher total HRR, more excess fuel will burn outside, and a higher flame height value is expected. This is confirmed in the results: regardless of the method used, the flame height value increases with the fire HRR. And the obtained results using 0.5 MW/m^3 are higher the using 1.2 MW/m^3. When using temperature based method, FDS over-predicts the external flame height with a maximum relative deviation of about 17.85%. When using HRRPUV based method (e.g., taking 1.2 MW/m^3 as reference value), FDS over-predicts the external flame height with a maximum relative deviation of about 24.51%. However, it is more important that trends are captured correctly. Indeed, there are important uncertainties when comparing flame heights: sensitivity on the exact choice of critical temperature or HRRPUV, as well as uncertainty on the correctness at the level of HRR inside the enclosure. Presuming some

Table 4
Comparison of Flame Height Between Simulation and Experiment for Opening Size of 0.2 m × 0.2 m

| Case no.	HRR_{Total} (kW)	Z_{f-exp} (m)	$Z_{f-hrrpuv}$ (1.2MW/m³) (m)	$Z_{f-hrrpuv}$ (0.5 MW/m³) (m)	Z_{f-tem} (520°C) /m	$(Z_{f-hrrpuv\,(1.2)} - Z_{f-exp})/Z_{f-exp}$ (%)	$(Z_{f-hrrpuv\,(0.5)} - Z_{f-exp})/Z_{f-exp}$ (%)	$(Z_{f-tem} - Z_{f-exp})/Z_{f-exp}$ (%)
11	60	0.70	0.87	1.09	0.81	24.51	56.00	15.71
8	50	0.56	0.67	0.77	0.66	20.52	38.51	17.85
31	40	0.40	0.45	0.58	0.46	12.74	45.30	15.00
32	30	0.34	0.37	0.49	0.37	9.38	44.85	8.82

under-prediction of the latter (see above), over-predictions of external flame heights are to be expected due to a higher fuel excess factor. As such, the deviations observed seem reasonable, in the authors' opinion.

Considering that the height of the flame ejected is mainly determined by two factors, namely the amount of excess fuel and the opening geometry of the enclosure, Lee proposed the following expression for external flame height Z_f in [6] [7]:

$$\frac{Z_f}{(A\sqrt{H})^{2/5}} = fcn\left[\frac{\dot{Q}_{ext}}{\rho_\infty C_P T_\infty \sqrt{g} A\sqrt{H}}\right] \tag{10}$$

where $\dot{Q}_{ext}$ is the external HRR, calculated as $\dot{Q}_{ext} = \dot{Q} - \dot{Q}_{in}$. The external flame height was recorded in [6, 7] by a CCD camera facing the façade. The flame tip was defined as the height where the flame presence probability is 50%. The flame height was measured from the neutral plane level at the opening, which is located at an approximate distance of $0.4H$ from the bottom of the opening [11].

Equation 10 and length scale $(A\sqrt{H})^{2/5}$ are used to analyze the flame height values obtained from FDS. In Figure 20, the crosses denote the experimental data, while the black dots represent the predicted simulation data. The trend line for all the simulation data, shown as a solid line, has a slope of 2/3 in this logarithmic scale plot: the power dependence for flame heights on the excess heat release rate is 2/3, which is similar to what is observed for wall fires [47, 48]. For large flame heights, the predictions show good agreement with the experimental data, while some under-prediction is observed for smaller flame heights.
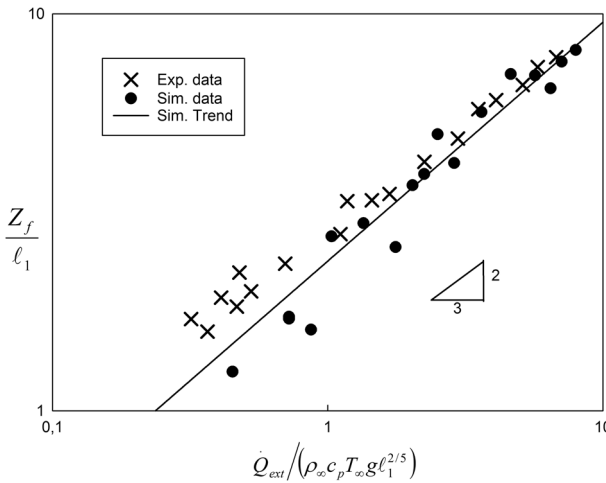
Figure 20. Comparion of flame heights obtained with FDS based on the temperature reference (520°C) method to experimental data using correlation (10).

4. Conclusion

Numerical simulations of under-ventilated enclosure fires with external flaming have been discussed. FDS, version 6.0.1, has been applied with the default settings. Four different opening geometries are considered: 0.1 m × 0.2 m, 0.2 m × 0.2 m, 0.2 m × 0.3 m, and 0.3 m × 0.3 m. There are 32 simulations in total. The accuracy of the results obtained has been discussed, comparing to experimental data [6, 7] and empirical correlations.

Due to the importance of the flow through the opening, the required fineness of the grid has been discussed by analyzing the mass balance 'error' based on post-processing of the output data. Two length scale ratios have been formulated, in addition to the classical D^* criterion for the fire source. The first ratio is the ventilation factor to the grid cell size $(\ell_1 = (A\sqrt{H})^{2/5}/\delta_x)$, while the second is the ratio of the hydraulic diameter of the opening to the grid cell size $(\ell_2^* = D_h/\delta_x)$. When these two length scales are larger than 10, the corresponding mass balance error is lower than 4%. The results in terms of velocities through the door opening and temperature in the door opening are then grid insensitive.

The air inflow rate through the opening is found to correlate linearly to the ventilation factor as $\dot{m} = C \cdot A\sqrt{H}$. The obtained C value is 0.41 which is at the low end of the range 0.4–0.6 found in the literature [15].The heat release rate inside the enclosure obtained from FDS show a linear relationship with the ventilation factor. The linear regression coefficient is 1130.7 kW/m$^{2.5}$, which is lower than the 'classical' value 1500 kW/m$^{2.5}$ value. This has been explained through the lower mass flow rate of incoming air and incomplete consumption of oxygen flowing into the compartment. There is also some uncertainty at the level of the experimental data, since the HRR inside the enclosure could not be measured directly.

The temperature predictions show that: (1) the temperature at back and front opposite corners are not identical, but a meaningful average temperature inside the enclosure can be defined, (2) the such obtained average gas temperatures inside the enclosure deviate <10% from Babrauskas' correlation [12, 26] for the different opening geometries.

FDS has been shown to accurately reproduce the neutral plane height for the various configurations. Two methods, namely a temperature based method and a volumetric heat release rate based method, were employed to define the flame height. The external flame height is over-predicted, which is in line with the presumed under-prediction of the heat release rate inside the enclosure (i.e., there is relatively more excess fuel, leading to combustion outside the enclosure). Moreover, there is sensitivity of the quantitative results on the choice of limit temperature and heat release rate per unit volume. Yet, the trends are captured correctly. The flame height value increases with the fire HRR. The power dependence of the flame height on excess heat release rate is 2/3.

Acknowledgments

References

1. Drysdale D (2011) An introduction to fire dynamics, 3rd edn. Wiley, New York
2. Bullen ML, Thomas PH (1979) Compartment fires with non-cellulosic fuels. In: 17th symposium (international) on combustion, The combustion Institute, Pittsburgh, pp 1139–1148
3. Kawagoe K (1958) Fire behaviour in rooms. Report of the building research institute, Japan, No 27
4. Harmathy TZ (1972) A new look at compartment fires. Fire Technol 8(3):196–217
5. Thomas PH, Heselden AJM (1972) Fully developed fires in single compartments, CIB Report No 20. Fire Research Note 923, Fir Research Station, Borehamwood, England
6. Lee YP, Delichatsios MA, Silcock G (2007) Heat Fluxes and Flame Heights in Facades from Fires in Enclosures of Varying Geometry. Proc Combust Inst 31:2521–2528
7. Lee YP (2006) Heat Fluxes and Flame Heights in External Façade Fires, Ph.D. thesis, University of Ulster, Fire SERT
8. Tang F, Hu LH, Delichatsios MA, Lu KH (2012) Experimental study on the flame height and temperature profile of buoyant window spill plume from an under-ventilated compartment fire. Int J Heat Mass Transf 55:93–101
9. Asimakopoulou EK, Kolaitis DI, Founti MA (2015) An experimental and numerical investigation of externally venting flames developing in an under-ventilated fire compartment-façade configuration. In: Proceedings of the European combustion meeting 2015
10. Fleischmann CM, Parkes AR (1997) Effect of ventilation on the compartment enhanced mass loss rate. In: Fire safety journal proceedings of the fifth international symposium, pp 415–426
11. Delichatsios MA, Silcock WH, Liu X, Delichatsios MM, Lee YP (2004) Mass pyrolysis rates and excess pyrolysate in fully developed enclosure. Fire Saf J 39:1–21
12. Babrauskas V, Williamson RB (1978) Post-flashover compartment fires: basis of a theoretical model. Fire Mater 2:39–53
13. Quintiere JG, DenBraven K (1978). Some theoretical aspects of fire induced flows through doorways in a room-corridor scale model. NBSIR 78–1512
14. Prahl J, Emmons HW (1975) Fire induced flow through an opening. Combust Flame 25:369–385
15. Rockett JA (1976) Fire induced gas flow in an enclosure. Combust. Sci. Technology 12:165–175
16. Thomas PH, Heselden AJM (1972). Fully Developed Fires in Single Compartments. Fire Research Note No.923. Fire Research Station, Borehamwood, England
17. Tanaka T, Nakaya I, Yoshida M (1985) Full scale experiments for determining the burning conditions to be applied to toxicity tests. In: Proceedings of the first international symposium on fire safety science, pp 129–38
18. Suard S, Koched A, Pretrel H, Audouin L (2015) Numerical simulations of fire-induced doorway flows in a small scale enclosure. Int J Heat Mass Transf 81:578–590

19. Stavrakakis GM, Markatos NC (2009) Simulation of airflow in one and two room enclosures containing a fire source. Int J Heat Mass Transf 52(11–12):2690–2703
20. Wang L, Lim J, Quintiere JG (2011) On the prediction of fire-induced vent flows using FDS. J Fire Sci 30:110–121
21. Chow WK, Zou GW (2005) Correlation equations on fire-induced air flow rates through doorway derived by large eddy simulation. Build Environ 40:897–906
22. Pretrel H, Koched A, Audouin L (2015) Doorway flows induced by the combined effects of natural and forced ventilation in case of multi-compartments large-scale fire experiments. Fire Technol 1–26
23. McGrattan K, Klein B, Hostikka S, Floyd J (2012) Fire dynamics simulator (version6), Users' Guide, National Institute of Standards and Technology Report NIST special publication
24. McGrattan K, Klein B, Hostikka S, Floyd J (2012) Fire dynamics simulator (version6), technical reference guide, National Institute of Standards and Technology Report NIST special publication
25. DiNenno PJ, et al. (Eds) SFPE Handbook of fire protection engineering, Chapter 6, Section 3, 2nd edn, 3, pp 134–147
26. Babrauskas V (1981) A closed-form approximation for post-flashover compartment fire temperatures. Fire Saf J 4:63–73
27. Floyd J, McGrattan K Validation of a CFD fire model using two step combustion chemistry using the NIST reduced-scale ventilation-limited compartment data, fire safety science. In: Proceedings of the ninth international symposium, pp 117–128
28. Tanga F, Hua LH (2012) Experimental study on flame height and temperature profile of buoyant window spill plume from an under-ventilated compartment fire. Int J Heat Mass Transf 55(1–3):93–101
29. Hu Z, Utiskul Y, Quintiere JG (2007) Towards large eddy simulations of flame extinction and carbon monoxide emission in compartment fires. Proc Combust Inst 31:2537–2545
30. Lecoustre V, Narayanan P, Baum HR, Trouve A (2011) Local Extinction of Diffusion Flames in Fires. Fire Saf Sci 10:583–595
31. Audouin L, Kolb G, Torero JL, Most JM (1995) Average centerline temperatures of a buoyant pool fire obtained by image processing of video recordings. Fire Saf J 24:167–187
32. Law M, O'Brien T (1989) Fire safety of bare external structural steel, The Steel Construction Institute, SCI Publication 009, U.K. ISBN: 0 86200 026 2
33. Oleszkiewicz I (1989) Heat transfer from a window fire plume to a building façade. Am Soc Mech Eng Heat Transf Div 123:163–170
34. Himotoa K, Tsuchihashib T et al (1995) Modeling the trajectory of window flames with regard to flow attachment to the adjacent wall. Fire Saf J 44(2):250–258
35. Goble K (2007) Height of flames projecting from compartment openings. Master thesis, University of Canterbury
36. Zhang J, Delichatsios MA, Colobert M, Hereid J (2008) Experimental and numerical investigations of heat impact and flame heights from fires in SBI tests. In: Fire safety science proceedings of the ninth international symposium, pp 205–216
37. Ma T, Quintiere JG (2001) Numerical Simulation of Axi-symmetric Fire Plumes: Accuracy and Limitations. MS Thesis, University of Maryland
38. Friday P, Mowrer FW (2001) Comparison of FDS Model Predictions with FM/SNL Fire Test Data'', NIST GCR 01–810. National Institute of Standards and Technology, Gaithersburg

39. McGrattan KB (2002) Improved radiation and combustion routines for a large eddy simulation fire model. In: Fire safety science, proceedings of the seventh international symposium, international association for fire safety science, WPI, Worcester, pp 827–838

40. Bounagui A (2003) Simulation of the fire for a section of the L.H. La fortaine tunnel, IRC-RR- 140. National Research Council Canada, Ottawa

41. Grosshandle W (2005) Report of the technical investigation of the station night club fire, NIST NCSTAR 2, 1National Institute Standards and Technology, Gaithersburg

42. McGrattan KB, Baum HR, Rehm RG (1998) Large Eddy Simulations of Smoke Movement. Fire Saf J 30(2):161–178

43. Heskestad G (1999) Flame Heights of Fuel Arrays with Combustion in Depth, Fire Safety Science.In: Proceeding of the Fifth International Symposium, pp 427–438

44. Lock A, Bundy M, et al. (2008) Experimental study of the effects of fuel type, fuel distribution, and vent size on full-scale under-ventilated compartment fires in an ISO 9705 room. NIST Technical Note 1603, pp. 53–54

45. Cox G (eds) (1995) Basic considerations, in combustion fundamentals of fire. Academic Press, London, pp 1–30

46. Orloff L, de Ris JN (1982) Froude modelling of pool fires. In: 19th Symposium (international) on combustion, The Combustion Institute, Pittsburgh, pp 885–895

47. Hasemi Y (1984) Experimental Wall Flame Heat Transfer Correlations for the analysis of Upward Wall Flame Spread. Fire Sci Technol 4:75–90

48. Quintiere J, Harkleroad M, Hasemi Y (1986) Wall flames and implications for upward flame spread. Combust Sci Technol 48(3–4):191–222